

## Article

# A Watt-Level, High-Quality $LG_{0,\pm 1}$ Vortex Beam made from a Nd:YVO<sub>4</sub> Laser Pumped by an Annular Beam

 Minghao Guo <sup>1,†</sup>, Xin Tao <sup>1,†</sup>, Yueqing Li <sup>1</sup>, Shirui Zhang <sup>1</sup>, Zhenkun Wu <sup>1,2</sup> , Yuzong Gu <sup>1,2</sup>  and Peng Li <sup>1,2,\*</sup> 

<sup>1</sup> Key Laboratory for High Efficiency Energy Conversion Science and Technology of Henan Province, School of Physics and Electronics, Henan University, Kaifeng 475004, China; guo\_mh2001@163.com (M.G.); taoxin0202@foxmail.com (X.T.); 15736888834@163.com (Y.L.); zhangsr925@163.com (S.Z.); wuzk1121@henu.edu.cn (Z.W.); yzgu@vip.henu.edu.cn (Y.G.)

<sup>2</sup> International Joint Research Laboratory of New Energy Materials and Devices of Henan Province, School of Physics and Electronics, Henan University, Kaifeng 475004, China

\* Correspondence: lilipengpeng@vip.henu.edu.cn

† These authors contributed equally to this work.

**Abstract:** In this work, we demonstrate a Watt-level, high-quality Laguerre–Gaussian (LG)  $LG_{0,\pm 1}$  vortex mode directly output from an end-pumped Nd:YVO<sub>4</sub> laser by using an axicon-based annular pump beam. A theoretical model for the annular beam end-pumped solid-state laser with an LG vortex mode output was established. Chirality control of the vortex laser was achieved by carefully tilting the output coupler. Watt-level 1064 nm lasers with pure  $LG_{0,1}/LG_{0,-1}$  vortex mode, and the incoherent superposition mode of  $LG_{0,1}$  odd and even petal modes, were achieved successively in our experiments. The intensity profile of the generated pure  $LG_{0,1}$  vortex laser was measured, and it can be well fitted by using the standard expression of the  $LG_{0,1}$  vortex mode. The beam quality of the pure  $LG_{0,1}$  mode is  $M_x^2 = 2.01$  and  $M_y^2 = 2.00$  along the  $x$ -axis and  $y$ -axis, respectively. Our study demonstrates that that axicon-based annular pumping has great potential in developing high-power vortex solid-state lasers with simple and compact structures.

**Keywords:** Nd:YVO<sub>4</sub> laser; axicon-based annular beam; vortex laser; chirality control



**Citation:** Guo, M.; Tao, X.; Li, Y.; Zhang, S.; Wu, Z.; Gu, Y.; Li, P. A Watt-Level, High-Quality  $LG_{0,\pm 1}$  Vortex Beam made from a Nd:YVO<sub>4</sub> Laser Pumped by an Annular Beam. *Photonics* **2024**, *11*, 843. <https://doi.org/10.3390/photonics11090843>

Received: 15 August 2024

Revised: 2 September 2024

Accepted: 3 September 2024

Published: 5 September 2024



**Copyright:** © 2024 by the authors. Licensee MDPI, Basel, Switzerland. This article is an open access article distributed under the terms and conditions of the Creative Commons Attribution (CC BY) license (<https://creativecommons.org/licenses/by/4.0/>).

## 1. Introduction

A vortex beam is a special annular optical field characterized by a helical phase wavefront, carrying orbital angular momentum (OAM) and having null intensity at the beam center [1]. It has widespread applications in various fields such as particle trapping [2], optical communications [3], super-resolution imaging [4], quantum optics [5], rotational Doppler effect [6], optical machining [7], multiple-star detections in astronomy [8], biomedicine and chemistry [9], etc. To meet the requirements of various application fields, there are increasing demands for vortex beams with a higher beam quality and mode purity.

As a typical vortex beam, the Laguerre–Gaussian (LG) laser mode  $LG_{p,l}$  with zero radial order ( $p = 0$ ) but nonzero azimuthal order ( $l \neq 0$ ) has attracted widespread interest in recent decades. Various methods, including passive and active schemes, have been demonstrated to generate the LG vortex beam. Passive methods entail converting the fundamental Gaussian or Hermite–Gaussian modes into LG modes by using a variety of designed optical components outside the laser resonator, such as ‘fork’ grating [10,11], inhomogeneous anisotropic media [12,13], a cylindrical lens pair [14,15], a spatial light modulator (SLM) [16–18], a digital micromirror device [19], a spiral phase plate (SPP) [20,21], q-plates [22], photon sieves [23], metasurfaces [24], etc. However, LG vortex beams generated by passive methods possess such drawbacks as poor beam quality, low conversion efficiency, transmission instability, wavelength sensitivity of the optical element, a low damage threshold, high production costs, and so on. Active methods involve directly generating the LG modes inside the laser cavity by controlling the intracavity modal gain

and loss, since LG beams are eigensolutions of the Helmholtz equation in cylindrical coordinates. Several active methods have been reported, including the use of annular pump light [25–52], off-axis pumping [53–57], thermal lensing [58–67], thermally induced birefringence [68,69], a dual cavity [70–72], anti-resonant rings [73,74], an unstable cavity [75], and inserting mode-selecting devices (intracavity amplitude elements: cavity mirrors with spot defects [76–79], circular absorber [80], amplitude mask element [81]; intracavity phase elements: spiral phase elements [82,83], phase plate [84], SLM [85]; intracavity spin–orbital coupling elements: q-plate [86,87], vortex wave plate [88], metasurface [89]). Among these methods, annular pumping has been proven to be an effective way to generate  $LG_{0,l}$  vortex beams, with advantages of high efficiency, high mode purity, high beam quality, and good stability, since the annular pump beam has the optimal spatial overlap with the  $LG_{0,l}$  mode. Shaping the pump light into the annular profile is usually accomplished by a circular diaphragm [25], a misaligned multi-mode fiber [26–30], a capillary fiber [31–38], a central hollow plane mirror [39,40], a hollow focus lens [41–44], circle Dammann grating [45,46], conical refraction [47], and an axicon [48–52]. An axicon combined with a focused lens can transform the Bessel beam into an annular beam efficiently [90]; thus, the axicon is an important commercially available optical element that can be utilized to reshape the pump beam into a ring-shaped profile with high efficiency (>90%) and wavelength insensitivity, and it only needs to be inserted into the pump unit in the LD end-pumped solid-state laser without affecting the structure of the laser resonator. However, the annular beam end-pumped solid-state laser may yield an output beam with a petal-pattern structure [26,27,52] that is a coherent superposition of two LG vortex modes of opposite handedness. Furthermore, the doughnut-shaped beam directly output from the laser may not be of real  $LG_{0,l}$  vortex mode but an incoherent superposition of two petal beams [91], although they have an identical transverse intensity distribution. Hence, robust direct generation of LG vortex beams with well-determined handedness (pure LG vortex mode) is desirable.

The selection of wavefront handedness has been achieved simply by inserting and tilting an etalon in the resonator [33,36], which breaks the propagation symmetry of the Poynting vectors with opposite helicity. However, this requires precise cavity alignment, and it involves a significant waste of output power due to insertion losses. It was demonstrated that slight tilting of the cavity can break the spiral propagation symmetry of two LG mode beams with opposite helical wavefronts, resulting in the selection of wavefront handedness [28,42,84]. Thus, tilting the cavity is an effective method to select the wavefront handedness of the output laser beam. The thermal effects of the laser crystal not only hinder the power scaling of the vortex laser, but also lead to the deterioration of beam quality [58–67]. So, it is quite difficult to achieve high-power and high-beam-quality vortex laser output simultaneously.

In this paper, we report the direct generation of a high-power and high-beam-quality pure  $LG_{0,\pm 1}$  vortex beam in an axicon-based annular beam end-pumped Nd:YVO<sub>4</sub> solid-state laser. Three kinds of laser modes (pure  $LG_{0,1}/LG_{0,-1}$  vortex mode, and the incoherent superposition mode between  $LG_{0,1}$  odd and even petal modes) with the same beam pattern (intensity distribution) can be switched by titling the output coupler. These three modes can be distinguished by the interferograms between the annular beam and its conjugate one. Section 2 presents the theoretical model for the output characteristics of the axicon-based annular beam end-pumped solid-state laser. Section 3 is devoted to the description of the experimental setup. The experimental results and simulations, including the beam patterns and topological charges (TCs) of the output laser, input–output relationship, and beam quality and polarization characteristics, are discussed in Section 4. Finally, the conclusion is presented in Section 5. This work provides an effective method for generating a stable pure LG vortex beam with high-mode-purity output from a compact, simple, and efficient solid-state laser.

## 2. Theoretical Model

For an axicon-based annular beam end-pumped solid-state laser, the threshold pump power ( $P_{th}$ ) for a single  $LG_{0,l}$  mode can be expressed as follows [92]:

$$P_{th}(LG_{0,l}) = \frac{hv_p\delta}{2\sigma L\tau_f\eta_t\eta_a\eta_p} \frac{1}{\iiint S_{0,l}(r,z)R_p(r,z)dV} \quad (1)$$

where  $h$  is Planck's constant,  $\delta = T + \delta_i$  represents the roundtrip loss of the laser resonator,  $T$  is the transmission loss of the output coupler, and  $\delta_i$  is the other losses, including diffraction loss, scattering loss, and absorption loss.  $\sigma$  is the emission cross-section of the gain medium,  $L$  is the optical length of the cavity,  $\tau_f$  is the fluorescence lifetime of the gain medium,  $\eta_a = 1 - [\exp(-\alpha_c l_c) + \exp(-\alpha_a l_c)]/2$  is the absorption ratio of pump power with the absorption coefficient  $\alpha_i$  ( $i = c$  for pump light polarized along the  $c$  axis,  $i = a$  for pump light polarized along the  $a$  axis) for the polarized-dependent absorption gain medium (such as  $a$ -cut Nd:YVO<sub>4</sub>) [93],  $l_c$  is the length of the gain medium,  $\eta_t$  is the optical transfer efficiency (the ratio between the incident pump power on the gain medium and that emitted by the pump source),  $\eta_p = v_l/v_p$  is the pump quantum efficiency, and  $v_p$  and  $v_l$  are pump and laser frequencies, respectively.  $S_{0,l}(r, z)$  is the normalized cavity mode intensity distribution.  $R_p(r, z)$  is the normalized pumping distribution in the laser crystal.

The normalized cavity mode intensity distribution  $S_{0,l}(r, z)$  for the  $l$ -th order LG mode can be expressed as follows:

$$S_{0,l}(r, z) = \frac{2}{\pi l_c w(z)^2 |l|!} \left[ \frac{2r^2}{w(z)^2} \right]^{|l|} \exp \left[ -\frac{2r^2}{w(z)^2} \right] \quad (2)$$

Here,  $w(z)$  is the beam radius of the fundamental mode of the  $LG_{0,l}$  mode.

The annular pump beam is obtained by Fourier transforming the Bessel Gaussian beam, which is generated by modulating the pump beam with an axicon [90]. Thus, the combination of an axicon and a lens is employed to reshape the pump beam. The normalized pumping distribution  $R_p(r, z)$  can be expressed by

$$R_p(r, z) = \frac{1}{\sqrt{2\pi}\pi\rho\Delta} \frac{\alpha_i \exp(-\alpha_i z)}{1 - \exp(-\alpha_i l_c)} \exp \left[ -\frac{2(r - \rho)^2}{\Delta^2} \right]. \quad (3)$$

Here,  $\rho$  represents the radius of the annular beam incident on the center of the laser crystal, while  $\Delta$  is the half-width of the annular beam. Since the gain medium is short, the variation in the annular pump beam distribution over the propagation distance is ignored here.

Substituting Equations (2) and (3) into Equation (1), the threshold pump power ( $P_{th}$ ) can be further expressed as

$$P_{th}(LG_{0,l}) = \frac{hv_p\delta}{2\sigma L\tau_f\eta_t\eta_a\eta_p} \frac{1}{f(\rho, \Delta, l)}, \quad (4)$$

where  $f_1(\rho, \Delta, l)$  is the mode overlap ratio between the annular pump beam and the LG laser mode; its specific form is

$$f_1(\rho, \Delta, l) = \iiint S_{0,l}(x, y, z)R_p(x, y, z)dV = \frac{4}{\sqrt{2\pi}\pi\rho\Delta l_c w_0^2 |l|!} \int_0^{+\infty} \exp \left[ -2 \left( \frac{(r - \rho)^2}{\Delta^2} + \frac{r^2}{w_0^2} \right) \right] \cdot \left( \frac{2r^2}{w_0^2} \right)^l r dr. \quad (5)$$

The laser mode with the lowest threshold pump power will oscillate in the laser resonator.

This is defined as

$$f_2(\rho, \Delta, l) = \iiint S_{0,l}^2(x, y, z) R_P(x, y, z) dV$$

$$= \frac{8}{\sqrt{2\pi}\pi^2 \rho \Delta l_c^2 w_0^4 (l!)^2} \int_0^{+\infty} \exp\left[-2\left(\frac{(r-\rho)^2}{\Delta^2} + \frac{2r^2}{w_0^2}\right)\right] \cdot \left(\frac{2r^2}{w_0^2}\right)^{2|l|} r dr \quad (6)$$

The output power is expressed as follows:

$$P_{out} = \eta_t \eta_a \eta_p \frac{T}{\delta} \frac{f_1^2}{f_2} (P_{in} - P_{th}) \quad (7)$$

### 3. Experimental Setup

The experimental setup for the axicon-based annular beam end-pumped LG vortex laser and the Mach–Zehnder interferometer (MZI)-based TC measurement is shown in Figure 1. A fiber-coupled laser diode (LD, BWT Ltd., Beijing, China) at 808 nm is selected as the pump source, with a maximum output of 30 W from a 400 μm diameter fiber. The pump beam is collimated by a lens  $L_1$  (DHC, GCX-L010-SMA-f40, Daheng Optics, Beijing, China) with a focal length of  $f = 40$  mm. The combination of the axicon (base angle  $\gamma = 1^\circ$ ) and lens  $L_2$  (focal length: 50 mm) converts the circular pump beam to the annular pump beam [90], which is focused on the center of the laser gain crystal in the subsequent experiment. The gain crystal is an a-cut 0.5 at.% Nd:YVO<sub>4</sub> crystal with a length of 5 mm and a cross-section of 5 mm × 5 mm. The front surface of the Nd:YVO<sub>4</sub> crystal, serving as an input coupler (IC), is an anti-reflection coating at a pump wavelength of 808 nm and a high-reflectivity (HR,  $R > 99.8\%$ ) coating at 1064 nm. The rear surface has high transmission (HT,  $T > 99\%$ ) at 1064 nm. The crystal wrapped in indium foil is mounted in a water-cooled copper block with a maintained water temperature of 17 °C. The laser resonator, composed of the IC (front surface of the Nd:YVO<sub>4</sub> crystal) and the output coupler (OC, a plane mirror with 1.5% transmission at 1064 nm and HT at 808 nm), is employed as the laser resonator. The OC is tilted to control the chirality of the output LG vortex beam. The movable diaphragm is inserted in the plane–plane resonator in order to prevent the oscillation of the Hermite–Gaussian modes while tilting the OC. The generated LG vortex beam and the transmitted 808 nm pump beam are then separated by dichroic mirrors  $DM_{1,2}$ .

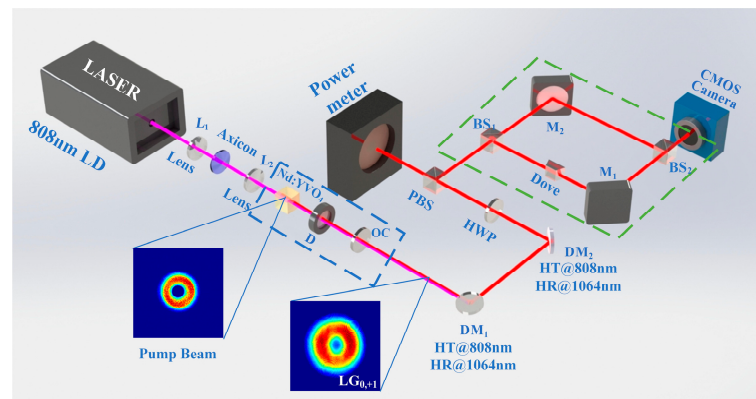


**Figure 1.** A schematic illustration of the axicon-based annular beam end-pumped Nd:YVO<sub>4</sub> LG vortex laser and the measurement of the TC. L: lens; D: diaphragm; OC: output coupler;  $DM_{1,2}$ : dichroic mirrors (high reflection,  $R > 99.5\%$  @ 1064 nm; high transmission,  $T > 95\%$  @ 808 nm); M: high-reflection mirrors; HWP: half-wave plate; PBS: polarizing beam splitter; BS: beam splitter. The blue box represents the resonator for the vortex laser, and the green box represents the MZI used to measure the TC carried by the vortex laser.

The output LG vortex beam is divided into two parts by the power control system, constructed by the half-wave plate (HWP) and the polarizing beam splitter (PBS). The

main part is measured by the power meter (Thorlabs, PM 100D, Newton, NJ, USA), and a small part is injected into the MZI to confirm the handedness of the LG vortex beam. The MZI, composed of  $M_1$ ,  $M_2$ ,  $BS_1$ , and  $BS_2$  (non-polarizing), is used to realize the off-axis interference between the vortex beam and its conjugate one. Here, the dove prism inserted in the MZI is used to convert the vortex beam of TC  $l$  to its conjugate one of TC  $-l$ . The interference patterns are recorded by using a CMOS camera (Duderstadt, Germany, CINOGY, CinCam, CMOS-1202). The fork-shaped pattern with  $2|l|$  fork number (the module of fringe difference between both ends of the fork) is formed [21,94]. The chirality is determined by the fork direction, upward for positive TC and downward for negative TC in our experiment.

Figure 2 illuminates the measured annular pump beam at the focal plane of lens  $L_2$ . As shown in Figure 2a, the annular pump beam exhibits excellent symmetry. The width ( $2\Delta$ ) and diameter ( $2\rho$ ) of the annular pump beam are estimated by simulating the experimental intensity distribution with a standard intensity distribution expression of the annular beam  $I_p(r) = I_0 \exp[-2(r - \rho)^2 / \Delta^2]$ , as shown in Figure 2b,c. The diameter ( $2\rho$ ) and width ( $2\Delta$ ) of the annular pump beam are estimated to be 0.76 mm and 0.42 mm, respectively.

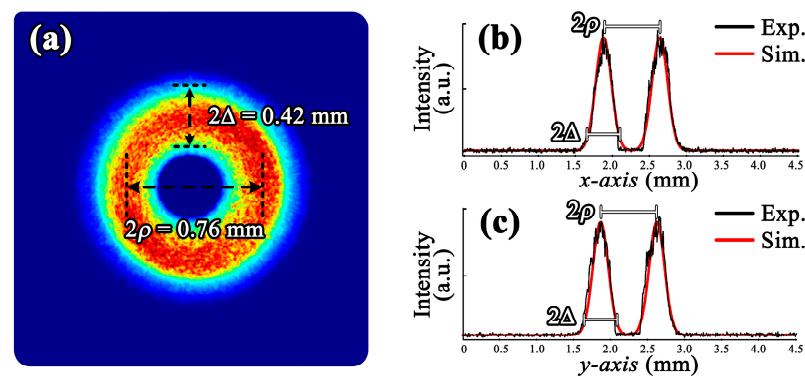


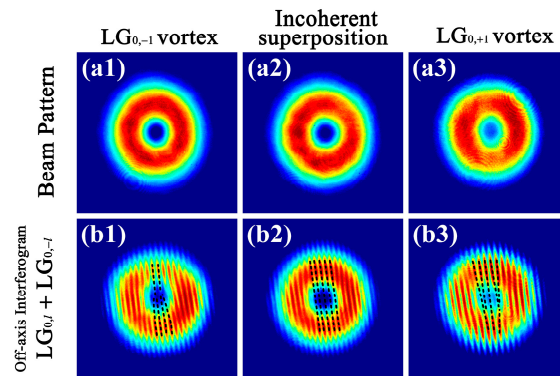
**Figure 2.** Annular pump beam profile. Beam pattern (a); intensity distributions along  $x$ -axis (b) and  $y$ -axis (c), respectively.

#### 4. Experimental Results and Discussion

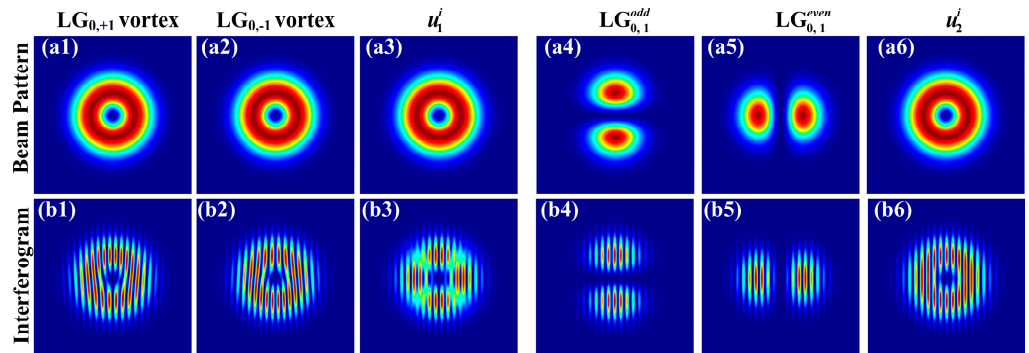
In the experiment, the annular pump beam distribution in the Nd:YVO<sub>4</sub> crystal can be slightly adjusted by changing the distance between the lens  $L_2$  and the laser crystal so that the annular laser beam can oscillate in the resonator. Three different kinds of laser modes oscillate in the resonator by titling the OC.

Figure 3 shows the beam patterns and corresponding interferograms of the output laser modes. As shown in Figure 3(a1–a3), the beam patterns for the three kinds of laser modes are similar, and we cannot distinguish these modes by beam patterns. The differences among these modes are phase singularities, which are determined by the interferograms between the annular beam and its conjugate one, as shown in Figure 3(b1–b3). As shown in Figure 3(b1), the fork at the beam center is formed by two fringes at the top and four fringes at the bottom for the fringes between the black dashed lines. The fork direction is downward, and the fork number is two. These results indicate that the laser mode is LG<sub>0,-1</sub> vortex mode. As shown in Figure 3(b3), the fork at the beam center is formed by five fringes at the top and three fringes at the bottom for the fringes between the black dashed lines. The fork direction is upward, and the fork number is two. These results suggest that the laser mode is LG<sub>0,+1</sub> vortex mode. We also notice that there exists a little difference for the fringe numbers in the black dashed lines of Figure 3(b1,b3). This is due to the phase difference  $\delta$  between the two interference beams. During the experiment, the phase difference  $\delta$  is affected by the optical path difference between two arms of the MZI, which is exposed to the air environment. By tilting the OC in the opposite direction, both LG<sub>0,1</sub> and LG<sub>0,-1</sub> vortex modes can oscillate in the laser resonator, as shown in Figure 3(a1,b1,a3,b3). The annular laser beam pattern shown in Figure 3(a2) is output from the laser when the laser

resonator is well closed. However, there exists no phase singularity in the annular beam, as shown in Figure 3(b2). The beam pattern shown in Figure 3(a2) may be formed by the following two situations: (i) the incoherent superposition mode ( $u_1^i$ ) of two pure LG vortex modes with opposite chirality ( $LG_{0,1}$  and  $LG_{0,-1}$ ); (ii) the incoherent superposition mode ( $u_2^i$ ) of  $LG_{0,1}$  odd and even petal modes. However, the interferograms between the annular beams and their conjugate ones are different for these two incoherent superposition modes, as shown in Figure 4. These two modes ( $u_1^i$  and  $u_2^i$ ) are different in the interferograms, as shown in Figure 4(b3,b6). These results demonstrate that the laser mode shown in Figure 3(b1–b3) of this manuscript is the incoherent superposition mode ( $u_2^i$ ) of  $LG_{0,1}$  odd and even petal modes. This is consistent with the previous report [91] that the output laser mode is known as the incoherent superposition mode of two petal beams.



**Figure 3.** The beam patterns (a1–a3) and corresponding interferograms (b1–b3) for different output laser modes. Columns 1, 2, and 3 show  $LG_{0,-1}$  vortex mode, the incoherent superposition mode of  $LG_{0,-1}$  vortex mode and  $LG_{0,-1}$  vortex mode, and  $LG_{0,+1}$  vortex mode, respectively.



**Figure 4.** The beam patterns (a1–a3) and corresponding interferograms between the beam and its conjugate one (b1–b3) for different laser modes. (a1,b1)  $LG_{0,1}$  vortex mode; (a2,b2)  $LG_{0,-1}$  vortex mode; (a3,b3) the incoherent superposition mode ( $u_1^i$ ) of two pure  $LG_{0,\pm 1}$  vortex modes; (a4,b4)  $LG_{0,1}^{odd}$  mode; (a5,b5)  $LG_{0,1}^{even}$  mode; (a6,b6) the incoherent superposition mode ( $u_2^i$ ) of  $LG_{0,1}$  odd and even modes.

The laser output power for three kinds of oscillation modes' operation as a function of incident pump power is plotted in Figure 5. Here, the circles are the experimental results, and the lines represent the simulation results. The threshold power was about 2.6 W, and the laser power increased nearly linearly with the incident pump power for the three kinds of modes. The laser yielded a maximum output power of 1.58 W for the incoherent superposition mode of  $LG_{0,1}$  and  $LG_{0,-1}$  vortex modes (green circles) at an incident power of 12.9 W, and the corresponding slope efficiency was 14.4%. When the output laser was fixed in  $LG_{0,-1}$  mode (blue circles), the output power was measured to be 1.09 W at an incident power of 11.2 W, with a corresponding slope efficiency of  $\sim 11.7\%$ . When the output laser was fixed in  $LG_{0,+1}$  mode (red circles), the output power was measured to be

0.94 W at an incident power of 10.3 W, with a corresponding slope efficiency of ~10.5%. These modes were stable during the variation in pump power shown here. The simulation results using the parameters shown in Table 1 agree well with the experimental ones. Here, the other losses are chosen to be  $\delta_1 = 5.50\%$  for the incoherent superposition modes, and  $\delta_2 = 6.90\%$  for the pure LG vortex mode, since the closure condition of the resonator is poor when the OC is tilted to output these pure vortex modes. The output power for the pure vortex modes of LG<sub>0,1</sub> and LG<sub>0,-1</sub> is lower than the output power for the incoherent superposition mode at any pump power.

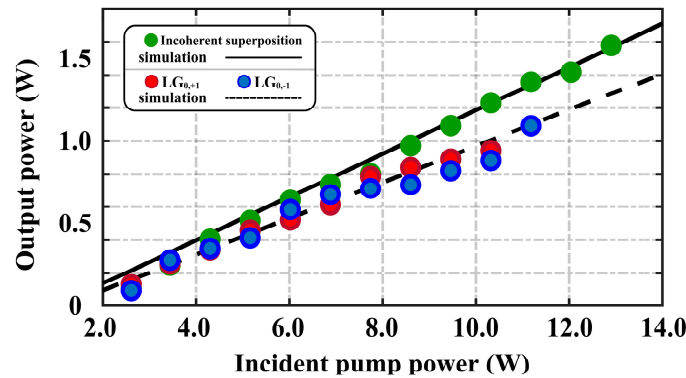


**Figure 5.** Output laser powers with respect to incident pump power for different vortex modes. Circles are experimental results, and lines represent simulation results using our theory.

**Table 1.** Simulation parameters in Figure 5.

$l_c$ (m)	$\sigma$ (m <sup>2</sup> )	$\tau_f$ (s)	$\alpha_1$ (cm <sup>-1</sup> )	$\alpha_2$ (cm <sup>-1</sup> )	$\eta_t$
$5 \times 10^{-3}$	$15.6 \times 10^{-23}$	$90 \times 10^{-6}$	8.8	2.4	100%
$\eta_p$	$w_0$ (mm)	$T$	$L$ (mm)	$\delta_1$ (solid line)	$\delta_2$ (dashed line)
75.94%	0.83	1.50%	20.00	5.50%	6.90%

The beam quality of the generated LG<sub>0,1</sub> vortex beam is studied. A plano-convex lens with a focal length of  $f = 200$  mm focuses the pure LG<sub>0,1</sub> vortex laser at a pump power of 5 W; the beam patterns and intensity distributions along the  $x$ - and  $y$ -axes of the vortex laser are recorded for different propagation distances  $z$  behind the lens.

Figure 6 presents the beam patterns of the LG<sub>0,1</sub> vortex beam at different propagation distances  $z$  behind the focusing lens. The annular ring-shaped beam intensity profile was maintained throughout the focal plane, indicating that the generated laser mode in the experiment possesses propagation invariance, with variation only in the scale of the spatial intensity distribution, since the Fourier transform of LG<sub>0,1</sub> mode coincides with itself. That is to say, the generated mode is an eigenmode of the laser resonator. The beam radius  $w$  of the LG<sub>0,1</sub> vortex beam at different propagation distances  $z$  is obtained by fitting the intensity distribution using the standard one of the LG<sub>0,1</sub> vortex beam. For example, as shown in Figure 7(a1,a2), the beam radii of the LG<sub>0,1</sub> vortex beam at the propagation distance  $z = 30$  mm are  $w_x = 621$   $\mu\text{m}$  along the  $x$ -axis and  $w_y = 632$   $\mu\text{m}$  along the  $y$ -axis. Beam radii as a function of propagation distance  $z$  are plotted in Figure 7(b1,b2). By fitting the experimental data of beam radii with the equation  $w(z) = w [1 + M^2(z - z_0)^2(\lambda/\pi w^2)^2]^{1/2}$ , the beam quality factor  $M^2$  can be obtained. Here,  $z_0$  is the position of the beam waist, and  $\lambda$  is the wavelength. As shown in Figure 7(b1,b2), the beam quality factors are  $M_x^2 = 2.01$  along the  $x$ -axis and  $M_y^2 = 2.00$  along the  $y$ -axis, respectively. The experimental results of beam quality factors are very close to the ideal case of  $M^2$  for the LG<sub>01</sub> vortex beam ( $|l| + 1 = 2$ ).

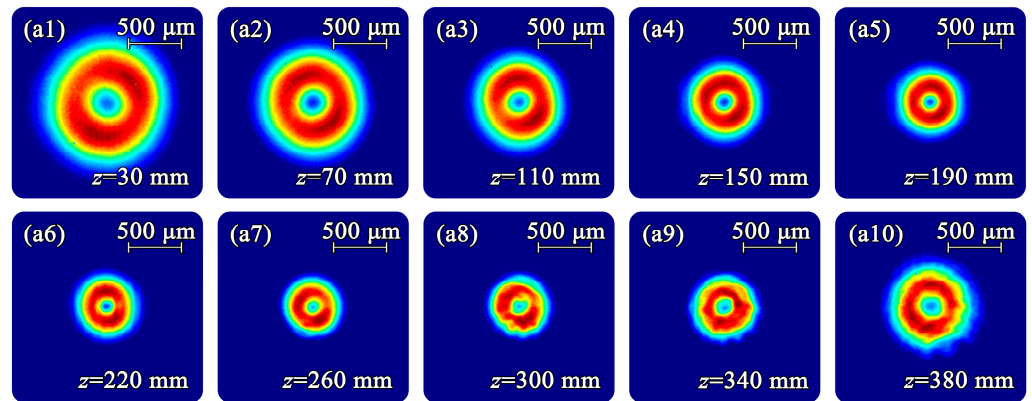


**Figure 6.** The beam patterns of the  $LG_{0,1}$  vortex beam for different propagation distances  $z$  behind the lens with a focal length of 200 mm at an incident pump power of 5 W. (a1)  $z = 30$  mm; (a2)  $z = 70$  mm; (a3)  $z = 110$  mm; (a4)  $z = 150$  mm; (a5)  $z = 190$  mm; (a6)  $z = 220$  mm; (a7)  $z = 260$  mm; (a8)  $z = 300$  mm; (a9)  $z = 340$  mm; (a10)  $z = 380$  mm.

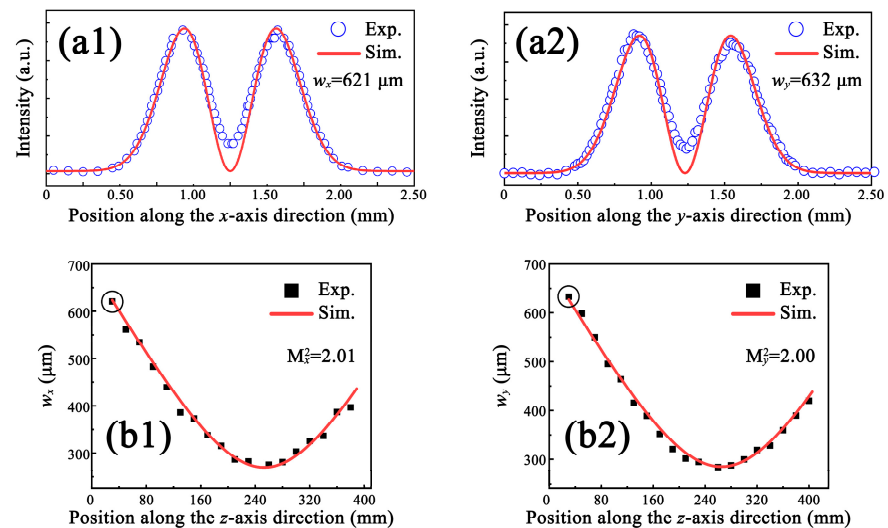


**Figure 7.** The intensity distributions and beam quality of the  $LG_{0,1}$  vortex beam. (a1,a2) The intensity distributions at the propagation distance  $z = 30$  mm. (b1,b2) The beam quality factor  $M^2$  along the  $x$ - and  $y$ -axes. The symbols and red solid curves stand for the measured data and fitting results, respectively.

The polarization state of the output vortex beam was also measured. By passing the  $LG_{0,1}$  vortex laser through the neutral optical attenuator and the rotated polarizer in sequence, the power transmitted to the polarizer is recorded by the power meter. Figure 8 plots the measured power (polarization state) versus the rotated angle of the polarizer. According to Figure 8b, the transmitted power varies sinusoidally with the rotation angle with the period of  $180^\circ$ . The minor axis is close to zero. It denotes an extinction of light when the polarizer is set at some special angles. Therefore, the generated  $LG_{0,1}$  vortex laser is determined to be linearly polarized. This is consistent with our expectation that the anisotropic gain medium (a-cut  $Nd:YVO_4$ ) tends to support linearly polarized laser oscillation.

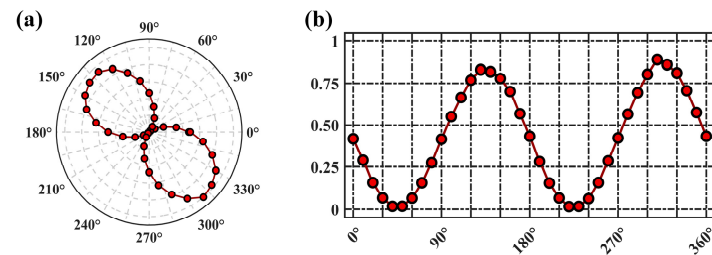


**Figure 8.** The polarization states of the output  $LG_{0,1}$  vortex beam at an incident pump power of 5 W. (a) Polar coordinate representation; (b) Cartesian coordinate representation.

## 5. Conclusions

In conclusion, we have studied the generation of the LG mode optical vortex beam in a Nd:YVO<sub>4</sub> laser end-pumped by an annular-shaped pump beam, which was generated by modulating the circular pump beam with the combination of an axicon and a lens. A simple theoretical model for the annular beam end-pumped solid-state laser was established. We have demonstrated that the tilted output coupler in the laser resonator can break the spiral propagation symmetry of two LG vortex mode beams with opposite helical wavefronts, resulting in the selection of wavefront handedness. Three kinds of laser modes (the pure  $LG_{0,\pm 1}$  vortex beam, the incoherent superposition mode of  $LG_{0,1}$  odd and even petal beams) with the same beam pattern (intensity distribution) can be output from the laser. A Watt-level, linear-polarized, pure  $LG_{0,\pm 1}$  vortex mode with high beam quality was generated in our experiment. The theoretical simulations for the output of the annular beam end-pumped solid-state laser using our theoretical model agreed well with the experimental results. These results indicate that it is a promising method to obtain a high-power pure  $LG_{0,\pm 1}$  vortex laser output from an axicon-based annular beam end-pumped solid-state laser by tilting the output coupler. However, the maximum output power was limited by the absorbed pump power. The use of a long gain medium in conjunction with a higher power pump beam should allow for scaling to much higher power for pure  $LG_{0,\pm 1}$  vortex laser beams.

**Author Contributions:** Conceptualization, M.G., X.T. and P.L.; investigation, M.G., X.T., Y.L. and S.Z.; data curation, M.G., X.T. and P.L.; writing—original draft preparation, M.G.; writing—review and editing, P.L., Z.W. and Y.G.; supervision, P.L.; funding acquisition, P.L. and Y.G. All authors have read and agreed to the published version of the manuscript.

**Funding:** This work was supported by the National Natural Science Foundation of China (NSFC) (12104131, 62375077, 61875053) and the Scientific and Technological Project in Henan Province (232102210170).

**Institutional Review Board Statement:** Not applicable.

**Informed Consent Statement:** Not applicable.

**Data Availability Statement:** The data will be made available on request.

**Conflicts of Interest:** The authors declare no conflicts of interest.

## References

- Allen, L.; Beijersbergen, M.W.; Spreeuw, R.J.C.; Woerdman, J.P. Orbital angular momentum of light and the transformation of Laguerre–Gaussian laser modes. *Phys. Rev. A* **1992**, *45*, 8185–8189. [[CrossRef](#)]
- Lavery, M.P.J.; Speirits, F.C.; Barnett, S.M.; Padgett, M.J. Detection of a spinning object using light’s orbital angular momentum. *Science* **2013**, *341*, 537–540. [[CrossRef](#)]
- Bozinovic, N.; Yue, Y.; Ren, Y.; Tur, M.; Kristensen, P.; Huang, H.; Willner, A.E.; Ramachandran, S. Terabit-scale orbital angular momentum mode division multiplexing in fibers. *Science* **2013**, *340*, 1545–1548. [[CrossRef](#)]
- Wang, B.; Shi, J.; Zhang, T.; Xu, X.; Cao, Y.; Li, X. Improved lateral resolution with an annular vortex depletion in STED microscopy. *Opt. Lett.* **2017**, *42*, 4885–4888. [[CrossRef](#)]
- Graffitti, F.; D’Ambrosio, V.; Proietti, M.; Ho, J.; Piccirillo, B.; De Lisio, C.; Marrucci, L.; Fedrizzi, A. Hyperentanglement in structured quantum light. *Phys. Rev. Res.* **2020**, *2*, 043350. [[CrossRef](#)]

6. Cheng, T.-Y.; Wang, W.-Y.; Li, J.-S.; Guo, J.-X.; Liu, S.; Lü, J.-Q. Rotational Doppler effect in vortex light and its applications for detection of the rotational motion. *Photonics* **2022**, *9*, 441. [[CrossRef](#)]
7. Toyoda, K.; Miyamoto, K.; Aoki, N.; Morita, R.; Omatsu, T. Using optical vortex to control the chirality of twisted metal nanostructures. *Nano Lett.* **2012**, *12*, 3645–3649. [[CrossRef](#)] [[PubMed](#)]
8. Aleksanyan, A.; Kravets, N.; Brasselet, E. Multiple-star system adaptive vortex coronagraphy using a liquid crystal light valve. *Phys. Rev. Lett.* **2017**, *118*, 203902. [[CrossRef](#)] [[PubMed](#)]
9. Jeffries, G.D.; Edgar, J.S.; Zhao, Y.; Shelby, J.P.; Fong, C.; Chiu, D.T. Using polarization-shaped optical vortex traps for single-cell nanosurgery. *Nano Lett.* **2007**, *7*, 415–420. [[CrossRef](#)]
10. Yang, F.F.; Li, H.; Liu, H.G.; Chen, X.F. Highly efficient nonlinear vortex beam generation by using a compact nonlinear fork grating. *Opt. Lett.* **2023**, *48*, 6376–6379. [[CrossRef](#)]
11. Soskin, M.; Vasnetsov, M.; Pas’ko, V.; Plutenko, D. Optical vortex generated with an asymmetric forked grating. *J. Opt.* **2020**, *22*, 104001. [[CrossRef](#)]
12. Marrucci, L.; Manzo, C.; Paparo, D. Optical spin-to-orbital angular momentum conversion in inhomogeneous anisotropic media. *Phys. Rev. Lett.* **2006**, *96*, 163905. [[CrossRef](#)]
13. Ling, X.H.; Luo, H.L.; Guan, F.X.; Zhou, X.X.; Luo, H.L.; Zhou, L. Vortex generation in the spin-orbit interaction of a light beam propagation inside a uniaxial medium: Origin and efficiency. *Opt. Express* **2020**, *28*, 27258–27267. [[CrossRef](#)]
14. Beijersbergen, M.W.; Allen, L.; Van der Veen, H.E.L.O.; Woerdman, J.P. Astigmatic laser mode converters and transfer of orbital angular momentum. *Opt. Commun.* **1993**, *96*, 123–132. [[CrossRef](#)]
15. Shen, D.H.; He, T.; Yu, X.B.; Zhao, D.M. Mode conversion and transfer of orbital angular momentum between Hermite-Gaussian and Laguerre-Gaussian beams. *IEEE Photonics J.* **2022**, *14*, 6510506. [[CrossRef](#)]
16. Ma, H.T.; Hu, H.J.; Xie, W.K.; Xu, X.J. Study on the generation of a vortex laser beam by using phase-only liquid crystal spatial light modulator. *Opt. Eng.* **2013**, *52*, 091721. [[CrossRef](#)]
17. Li, R.; Ren, Y.; Liu, T.; Wang, C.; Liu, Z.; Zhao, J.; Sun, R.; Wang, Z. Generating large topological charge Laguerre-Gaussian beam based on 4 k phase-only spatial light modulator. *Chin. Opt. Lett.* **2022**, *20*, 120501. [[CrossRef](#)]
18. Pinnell, J.; Rodríguez-Fajardo, V.; Forbes, A. Probing the limits of orbital angular momentum generation and detection with spatial light modulators. *J. Opt.* **2021**, *23*, 015602. [[CrossRef](#)]
19. Ren, Y.X.; Li, M.; Huang, K.; Wu, J.G.; Gao, H.F.; Wang, Z.Q.; Li, Y.M. Experimental generation of Laguerre-Gaussian beam using digital micromirror device. *Appl. Opt.* **2010**, *49*, 1838–1844. [[CrossRef](#)]
20. Beijersbergen, M.W.; Coerwinkel, R.P.C.; Kristensen, M.; Woerdman, J.P. Helical-wavefront laser beams produced with a spiral phaseplate. *Opt. Commun.* **1994**, *112*, 321–327. [[CrossRef](#)]
21. Zhou, Z.H.; Li, P.; Ma, J.B.; Zhang, S.R.; Gu, Y.Z. Generation and detection of optical vortices with multiple cascaded spiral phase plates. *Photonics* **2022**, *9*, 354. [[CrossRef](#)]
22. Rafayelyan, M.; Brasselet, E. Laguerre-Gaussian modal q-plates. *Opt. Lett.* **2017**, *42*, 1966–1969. [[CrossRef](#)] [[PubMed](#)]
23. Huang, K.; Liu, H.; Garcia-Vidal, F.J.; Hong, M.H.; Luk’yanchuk, B.; Teng, J.; Qiu, C.W. Ultrahigh-capacity non-periodic photon sieves operating in visible light. *Nat. Commun.* **2015**, *6*, 7059. [[CrossRef](#)]
24. Ahmed, H.; Kim, H.; Zhang, Y.B.; Intaravanne, Y.; Jang, J.; Rho, J.; Chen, S.Q.; Chen, X.Z. Optical metasurfaces for generating and manipulating optical vortex beams. *Nanophotonics* **2022**, *11*, 941–956. [[CrossRef](#)]
25. Chen, Y.F.; Lan, Y.P.; Wang, S.C. Generation of Laguerre-Gaussian modes in fiber-coupled laser diode end-pumped lasers. *Appl. Phys. B* **2001**, *72*, 167–170. [[CrossRef](#)]
26. Chen, Y.F.; Lan, Y.P. Dynamics of the Laguerre Gaussian TEM<sub>0,l</sub> mode in a solid state laser. *Phys. Rev. A* **2001**, *63*, 063807. [[CrossRef](#)]
27. Fang, Z.Q.; Yao, Y.; Xia, K.G.; Li, J.L. Simple Nd:YAG laser generated vector and vortex beam. *Chin. Opt. Lett.* **2015**, *13*, 031405. [[CrossRef](#)]
28. Fang, Z.Q.; Xia, K.G.; Yao, Y.; Li, J.L. Radially polarized LG<sub>01</sub>-mode Nd:YAG laser with annular pumping. *Appl. Phys. B* **2014**, *117*, 219–224. [[CrossRef](#)]
29. Fang, Z.Q.; Xia, K.G.; Yao, Y.; Li, J.L. Radially polarized and passively Q-switched Nd:YAG laser under annular-shaped pumping. *IEEE J. Sel. Top. Quant.* **2014**, *21*, 337–342. [[CrossRef](#)]
30. Bisson, J.F.; Senatsky, Y.; Ueda, K.I. Generation of Laguerre-Gaussian modes in Nd:YAG laser using diffractive optical pumping. *Laser Phys. Lett.* **2005**, *2*, 327. [[CrossRef](#)]
31. Kim, J.W.; Mackenzie, J.I.; Hayes, J.R.; Clarkson, W.A. High power Er:YAG laser with radially-polarized Laguerre-Gaussian (LG<sub>01</sub>) mode output. *Opt. Express* **2011**, *19*, 14526–14531. [[CrossRef](#)] [[PubMed](#)]
32. Kim, J.W. High-power laser operation of the first-order Laguerre-Gaussian (LG) mode in a diode-laser-pumped Nd:YAG laser. *J. Korean Phys. Soc.* **2012**, *61*, 739–743. [[CrossRef](#)]
33. Kim, D.J.; Kim, J.W.; Clarkson, W.A. Q-switched Nd:YAG optical vortex lasers. *Opt. Express* **2013**, *21*, 29449–29454. [[CrossRef](#)] [[PubMed](#)]
34. Kim, J.W.; Clarkson, W.A. Selective generation of Laguerre-Gaussian (LG<sub>0n</sub>) mode output in a diode-laser pumped Nd:YAG laser. *Opt. Commun.* **2013**, *296*, 109–112. [[CrossRef](#)]
35. Lin, D.; Daniel, J.M.O.; Clarkson, W.A. Controlling the handedness of directly excited Laguerre-Gaussian modes in a solid-state laser. *Opt. Lett.* **2014**, *39*, 3903–3906. [[CrossRef](#)]

36. Kim, D.J.; Kim, J.W. Direct generation of an optical vortex beam in a single frequency Nd:YVO<sub>4</sub> laser. *Opt. Lett.* **2015**, *40*, 399–402. [[CrossRef](#)]
37. Dietrich, T.; Rumpel, M.; Graf, T.; Ahmed, M.A. Investigations on ring-shaped pumping distributions for the generation of beams with radial polarization in an Yb:YAG thin-disk laser. *Opt. Express* **2015**, *23*, 26651–26659. [[CrossRef](#)]
38. Lu, J.L.; Lin, H.; Zhang, G.; Li, B.; Zhang, L.; Lin, Z.; Chen, Y.; Petrov, V.; Chen, W. Direct generation of an optical vortex beam from a diode-pumped Yb:MgWO<sub>4</sub> laser. *Laser Phys. Lett.* **2017**, *14*, 085878. [[CrossRef](#)]
39. Zhao, Y.; Liu, Q.; Zhou, W.; Shen, D. ~1 mJ pulsed vortex laser at 1645 nm with well-defined helicity. *Opt. Express* **2016**, *24*, 15596–15602. [[CrossRef](#)]
40. Liu, Q.; Zhao, Y.; Zhou, W.; Shen, D. Vortex operation in Er:LuYAG crystal laser at ~1.6 μm. *Opt. Mater.* **2017**, *71*, 31–34. [[CrossRef](#)]
41. He, H.S.; Chen, Z.; Dong, J. Direct generation of vector vortex beams with switchable radial and azimuthal polarizations in a monolithic Nd:YAG microchip laser. *Appl. Phys. Express* **2017**, *10*, 052701. [[CrossRef](#)]
42. He, H.S.; Chen, Z.; Li, H.B.; Dong, J. Low-threshold, nanosecond, high-repetition-rate vortex pulses with controllable helicity generated in Cr, Nd:YAG self-Q-switched microchip laser. *Laser. Phys.* **2018**, *28*, 055802. [[CrossRef](#)]
43. Chen, D.M.; Wang, X.C.; He, H.S.; Dong, J. Vector vortices with tunable polarization states directly generated in a microchip laser. *Appl. Phys. Express* **2019**, *12*, 052012. [[CrossRef](#)]
44. Chen, D.M.; Cai, S.; Dong, J. Highly efficient Yb: YAG microchip laser for direct generation of radially polarized vector vortices. *Eng. Res. Express* **2020**, *2*, 045035. [[CrossRef](#)]
45. Li, J.L.; Yao, Y.; Yu, J.J.; Xia, K.G.; Zhou, C.H. Efficient vortex laser with annular pumping formed by circle Damman grating. *IEEE Photonic Technol. Lett.* **2015**, *28*, 473–476. [[CrossRef](#)]
46. Xu, Y.; Han, X.H.; Li, G.Y.; Liu, J.Y.; Xia, K.G.; Li, J.L. Vortex and LG<sub>01</sub>-mode Nd:YAG laser involving a circular Damman grating. *Opt. Eng.* **2016**, *55*, 056101. [[CrossRef](#)]
47. Li, G.Y.; Xia, K.G.; Wang, Z.Y.; Shen, H.; Shirakawa, A.; Ueda, K.I.; Li, J.L. Conical refraction, for annular pumping of an efficient vortex Nd:YAG laser. *Laser Phys. Lett.* **2017**, *14*, 075001. [[CrossRef](#)]
48. Li, K.; Tang, K.F.; Lin, D.; Wang, J.; Li, B.X.; Liao, W.B.; Lin, Z.L.; Zhang, G. Direct generation of optical vortex beams with tunable topological charges up to 18th using an axicon. *Opt. Laser Technol.* **2021**, *143*, 107339. [[CrossRef](#)]
49. Liu, J.; Gu, J.; Huang, L.; Zhang, C.X.; Bai, Z.Y.; Fan, D.Y. Mid-infrared vortex array generation with a tunable singularity in an Er:YAP laser. *Appl. Phys. Lett.* **2023**, *123*, 021110. [[CrossRef](#)]
50. Fan, L.; Wang, L.M.; Sun, R.; Fan, H.B.; Zhu, J. High-power and efficient vortex Nd: YVO<sub>4</sub> laser using annular pumping. *Laser Phys.* **2023**, *33*, 115002. [[CrossRef](#)]
51. Liu, J.; Duan, Y.M.; Mao, W.J.; Jin, X.X.; Li, Z.H.; Zhu, H.Y. An axicon-based annular pump acousto-optic Q-switched Nd: GdVO<sub>4</sub> self-Raman vortex laser. *Crystals* **2023**, *13*, 1484. [[CrossRef](#)]
52. Zhang, Z.H.; Liu, J.; Duan, Y.M.; Zhang, Y.C.; Jin, X.X.; Li, Z.H.; Zhu, H.Y. Robust high-order petal-mode laser with tunable topological pumped by an axicon-based annular beam. *Appl. Phys. Lett.* **2024**, *124*, 151102. [[CrossRef](#)]
53. Huang, X.; Xu, B.; Cui, S.; Xu, H.; Cai, Z.; Chen, L. Direct generation of vortex laser by rotating induced off-axis pumping. *IEEE J. Sel. Top. Quant.* **2018**, *24*, 1601606. [[CrossRef](#)]
54. Lin, G.P.; Cao, Y.Q.; Ji, R.R.; Hou, C.F.; Lu, Z.H. Direct generation of a narrow-linewidth Laguerre–Gaussian vortex laser in a monolithic nonplanar oscillator. *Opt. Lett.* **2018**, *43*, 4164. [[CrossRef](#)] [[PubMed](#)]
55. Luo, S.Y.; Cai, Z.P.; Sheng, C.X.; Li, L.; Chen, Q. 604-nm high-order vortex beams directly generated from a Pr:YLF laser with a cavity-loss-induced gain switching mechanism. *Opt. Laser Technol.* **2020**, *127*, 106185. [[CrossRef](#)]
56. Lin, X.; Feng, Q.; Zhu, Y.; Ji, S.; Xiao, B.; Xu, H.; Li, W.; Cai, Z. Diode-pumped wavelength-switchable visible Pr<sup>3+</sup>:YLF laser and vortex laser around 670 nm. *Opto-Electron. Adv.* **2021**, *4*, 210006. [[CrossRef](#)]
57. Li, Q.; Xu, M.M.; Hu, M.; Li, H.Z.; Liu, C.; Ji, Y.Y.; Bi, M.H.; Zhou, X.F.; Ye, Z.B.; Liu, C. Direct generation of vortex beams from an off-axis pumped all-solid-state laser. *Opt. Quant. Electron.* **2024**, *56*, 699. [[CrossRef](#)]
58. Okida, M.; Omatsu, T.; Itoh, M.; Yatagai, T. Direct generation of high power Laguerre-Gaussian output from a diode-pumped Nd: YVO<sub>4</sub> 1.3-μm bounce laser. *Opt. Express* **2007**, *15*, 7616–7622. [[CrossRef](#)]
59. Okida, M.; Hayashi, Y.; Omatsu, T.; Hamazaki, J.; Morita, R. Characterization of 1.06 μm optical vortex laser based on a side-pumped Nd: GdVO<sub>4</sub> bounce oscillator. *Appl. Phys. B* **2009**, *95*, 69–73. [[CrossRef](#)]
60. Chard, P.; Shardlow, P.C.; Damzen, M.J. High-power non-astigmatic TEM<sub>00</sub> and vortex mode generation in a compact bounce laser design. *Appl. Phys. B* **2009**, *97*, 275. [[CrossRef](#)]
61. Zhao, Y.; Wang, Z.; Yu, H.; Zhuang, S.; Zhang, H.; Xu, X.; Xu, J.; Wang, J. Direct generation of optical vortex pulses. *Appl. Phys. Lett.* **2012**, *101*, 031113. [[CrossRef](#)]
62. Yao, Y.; Xia, K.; Kang, M.; Fang, Z.; Li, J. Transverse mode transition and LG<sub>01</sub>-mode generation in an end-pumped Nd: YVO<sub>4</sub> laser. *Chin. Opt. Lett.* **2013**, *11*, 121406. [[CrossRef](#)]
63. Ding, Y.; Xu, M.; Zhao, Y.; Yu, H.; Zhang, H.; Wang, Z.; Wang, J. Thermally driven continuous-wave and pulsed optical vortex. *Opt. Lett.* **2014**, *39*, 2366–2369. [[CrossRef](#)] [[PubMed](#)]
64. Wang, S.; Zhang, S.; Qiao, H.; Li, P.; Hao, M.; Yang, H.; Xie, J.; Feng, G.; Zhou, S. Direct generation of vortex beams from a double-end polarized pumped Yb:KYW laser. *Opt. Express* **2018**, *26*, 26925–26932. [[CrossRef](#)]
65. Zhang, W.Y.; Tong, L.Y.; Yuan, Y.; Chen, C.D.; Cai, Y.J.; Zhao, L.N. Self-Q-switched Tm: YAP vortex laser by thermal-lensing effect. *Infrared. Phys. Technol.* **2022**, *123*, 104197. [[CrossRef](#)]

66. Zhang, Z.L.; Gui, K.; Zhao, C.M.; Zhang, H.Y.; Xing, Y.X. Direct generation of vortex beam with a dual-polarization microchip laser. *IEEE Photonic Technol. Lett.* **2019**, *31*, 1221–1224. [[CrossRef](#)]
67. Lin, X.J.; Cui, S.W.; Ji, S.H.; Tian, Q.Y.; Zhu, Y.; Li, W.S.; Xu, H.Y.; Cai, Z.P. LD-pumped high-power high-efficiency orange vortex  $\text{Pr}^{3+}$ :YLF lasers. *Opt. Laser Technol.* **2021**, *133*, 106571. [[CrossRef](#)]
68. Yonezawa, K.; Kozawa, Y.; Sato, S. Generation of a radially polarized laser beam by use of the birefringence of a c-cut Nd:YVO<sub>4</sub> crystal. *Opt. Lett.* **2006**, *31*, 2151–2153. [[CrossRef](#)]
69. Ito, A.; Kozawa, Y.; Sato, S. Selective oscillation of radially and azimuthally polarized laser beam induced by thermal birefringence and lensing. *J. Opt. Soc. Am. B* **2009**, *26*, 708–712. [[CrossRef](#)]
70. Kim, D.J.; Kim, J.W. High-power TEM<sub>00</sub> and Laguerre-Gaussian mode generation in double resonator configuration. *Appl. Phys. B* **2015**, *121*, 401–405. [[CrossRef](#)]
71. Kim, D.J.; Mackenzie, J.I.; Kim, J.W. Adaptable beam profiles from a dual-cavity Nd:YAG laser. *Opt. Lett.* **2016**, *41*, 1740–1743. [[CrossRef](#)] [[PubMed](#)]
72. Kim, D.J.; Kim, J.W. Dual-cavity Nd:YAG laser with Laguerre-Gaussian (LG<sub>0n</sub>) mode output. *Opt. Commun.* **2017**, *383*, 26–30. [[CrossRef](#)]
73. Kerridge-Johns, W.R.; Damzen, M.J. Vortex laser from anti-resonant ring coupled cavities. *Opt. Express* **2018**, *26*, 32839–32846. [[CrossRef](#)] [[PubMed](#)]
74. Munj, A.H.; Kerridge-Johns, W.R. Unidirectional ring vortex laser using a wedge-plate shearing interferometer. *Opt. Express* **2023**, *31*, 4954–4963. [[CrossRef](#)] [[PubMed](#)]
75. Yan, R.P.; Li, M.M.; Li, X.D.; Zhao, C.; Zhou, Y.P.; Jiang, Y.G. Vortex laser generation and chirality control in a LD end pumped Nd:YVO<sub>4</sub> laser. *Optik* **2021**, *236*, 166669. [[CrossRef](#)]
76. Ito, A.; Kozawa, Y.; Sato, S. Generation of hollow scalar and vector beams using a spot-defect mirror. *J. Opt. Soc. Am. A* **2010**, *27*, 2072–2077. [[CrossRef](#)]
77. Tan, S.W.; Zhou, C.H.; Shirakawa, A.; Ueda, K.I.; Li, J.L. Vortex Ti: Sapphire laser by using an intracavity spot-defect spatial filter. *Opt. Laser Technol.* **2017**, *96*, 76–80. [[CrossRef](#)]
78. Qiao, Z.; Xie, G.Q.; Wu, Y.H.; Yuan, P.; Ma, J.G.; Qian, L.J.; Fan, D.Y. Generation high-charge optical vortices directly from laser up to 288th order. *Laser Photonics Rev.* **2018**, *12*, 1800019. [[CrossRef](#)]
79. Chen, H.; Li, X.W.; Cui, Y.F.; Zhang, B.Y.; Chang, X.Y.; Qi, Y.Y.; Ding, J.; Yan, B.Z.; Wang, Y.L.; Lu, Z.W.; et al. Generation of tunable vortex beams from a side-pumped Nd:YAG laser utilizing spot defect mirrors. *Opt. Commun.* **2024**, *563*, 130587. [[CrossRef](#)]
80. Harris, M.; Hill, C.A.; Tapster, P.R.; Vaughan, J.M. Laser modes with helical wave fronts. *Phys. Rev. A* **1994**, *49*, 3119. [[CrossRef](#)]
81. Hu, A.J.; Lei, J.; Chen, P.F.; Wang, Y.; Li, S.M. Numerical investigation on the generation of high-order Laguerre–Gaussian beams in end-pumped solid-state lasers by introducing loss control. *Appl. Opt.* **2014**, *53*, 7845–7853. [[CrossRef](#)]
82. Oron, R.; Danziger, Y.; Davidson, N.; Friesem, A.A.; Hasman, E. Laser mode discrimination with intra-cavity spiral phase elements. *Opt. Commun.* **1999**, *169*, 115–121. [[CrossRef](#)]
83. Oron, R.; Davidson, N.; Friesem, A.A.; Hasman, E. Efficient formation of pure helical laser beams. *Opt. Commun.* **2000**, *182*, 205–208. [[CrossRef](#)]
84. Yang, T.L.; Yang, J.; Li, X.P.; Wang, H.; Zhang, Z.Z.; Wang, Y.P.; Wang, X.J. High power nanosecond optical vortex laser oscillation in mode-selection slab resonator. *Appl. Phys. B* **2024**, *130*, 92. [[CrossRef](#)]
85. Ngcobo, S.; Litvin, I.; Burger, L.; Forbes, A. A digital laser for on-demand laser modes. *Nat. Commun.* **2013**, *4*, 2289. [[CrossRef](#)]
86. Naidoo, D.; Roux, F.S.; Dudley, A.; Litvin, I.; Piccirillo, B.; Marrucci, L.; Forbes, A. Controlled generation of higher-order Poincaré sphere beams from a laser. *Nat. Photonics* **2016**, *10*, 327–332. [[CrossRef](#)]
87. Zhou, W.; Bao, Y.S.; Xu, H.W.; Liu, J.; Cai, Y.; Xu, S.X.; Fan, D.Y. Highly efficient solid-state vortex laser in a robust and simple configuration. *Opt. Express* **2024**, *32*, 24156–24165. [[CrossRef](#)]
88. Wei, D.Z.; Cheng, Y.; Ni, R.; Zhang, Y.; Hu, X.P.; Zhu, S.N.; Xiao, M. Generating controllable Laguerre-Gaussian laser modes through intracavity spin-orbital angular momentum conversion of light. *Phys. Rev. Appl.* **2019**, *11*, 014038. [[CrossRef](#)]
89. Sroor, H.; Huang, Y.W.; Sephton, B.; Naidoo, D.; Vallés, A.; Ginis, V.; Qiu, C.W.; Ambrosio, A.; Capasso, F.; Forbes, A. High-purity orbital angular momentum states from a visible metasurface laser. *Nat. Photonics* **2020**, *14*, 498–503. [[CrossRef](#)]
90. Tao, X.; Liang, Y.; Zhang, S.R.; Li, Y.Q.; Guo, M.H.; Li, P. Generation of Perfect Vortex Beams with Complete Control over the Ring Radius and Ring Width. *Photonics* **2023**, *10*, 1382. [[CrossRef](#)]
91. Litvin, I.A.; Ngcobo, S.; Naidoo, D.; Ait-Ameur, K.; Forbes, A. Doughnut laser beam as an incoherent superposition of two petal beams. *Opt. Lett.* **2014**, *39*, 704–707. [[CrossRef](#)] [[PubMed](#)]
92. Kubodera, K.; Otsuka, K. Single-transverse-mode LiNdP<sub>4</sub>O<sub>12</sub> slab waveguide laser. *J. Appl. Phys.* **1979**, *50*, 653. [[CrossRef](#)]
93. McDonagh, L.; Wallenstein, R.; Knappe, R.; Nebel, A. High-efficiency 60 W TEM<sub>00</sub> Nd:YVO<sub>4</sub> oscillator pumped at 888 nm. *Opt. Lett.* **2006**, *31*, 3297–3299. [[CrossRef](#)] [[PubMed](#)]
94. Ma, J.; Li, P.; Zhou, Z.; Gu, Y. Characteristics of fork-shaped fringes formed by off-axis interference of two vortex beams. *J. Opt. Soc. Am. A* **2021**, *38*, 115–123. [[CrossRef](#)]

**Disclaimer/Publisher’s Note:** The statements, opinions and data contained in all publications are solely those of the individual author(s) and contributor(s) and not of MDPI and/or the editor(s). MDPI and/or the editor(s) disclaim responsibility for any injury to people or property resulting from any ideas, methods, instructions or products referred to in the content.